



Research paper

Dual sgRNA-directed tyrosinases knockout using CRISPR/Cas9 technology in Pacific oyster (*Crassostrea gigas*) reveals their roles in early shell calcification

Qian Li^a, Hong Yu^a, Qi Li^{a,b,*}

^a Key Laboratory of Mariculture, Ministry of Education, Ocean University of China, Qingdao 266003, China

^b Laboratory for Marine Fisheries Science and Food Production Processes, Qingdao National Laboratory for Marine Science and Technology, Qingdao 266237, China



ARTICLE INFO

Edited by: Marco Barucca

Keywords:

Crassostrea gigas
Shell formation
Calcification
CRISPR/Cas9
Tyrosinase

ABSTRACT

Biom mineralization processes in bivalves, particularly the initial production of molecular components (such as matrix deposition and calcification) in the early stages of shell development are highly complex and well-organized. This study investigated the temporal dynamics of organic matrix and calcium carbonate (CaCO₃) deposition in Pacific oysters (*Crassostrea gigas*) across various development stages. The shell-field initiated matrix secretion during the gastrula stage. Subsequent larval development triggered central shell-field calcification, accompanied by expansion of the calcium ring from its interior to the periphery. Notably, the expression patterns of *CgTyrp-2* and *CgTyr* closely correlated with matrix deposition and calcification during early developmental stages, with peak expression occurring in oyster's gastrula and D-veliger stages. Subsequently, the CRISPR/Cas9 system was utilized to knock out *CgTyrp-2* and *CgTyr* with more distinct phenotypic alterations observed when both genes were concurrently knocked out. The relative gene expression was analyzed post-knockout, indicating that the knockout of *CgTyr* or *CgTyrp-2* led to reduced expression of *CgChs1*, along with increased expression of *CgChit4*. Furthermore, when dual-sgRNAs were employed to knockout *CgTyrp-2*, a large deletion (2 kb) within the *CgTyrp-2* gene was identified. In summary, early shell formation in *C. gigas* is the result of a complex interplay of multiple molecular components with *CgTyrp-2* and *CgTyr* playing key roles in regulating CaCO₃ deposition.

1. Introduction

The shell, the central protective structure for shellfish, serves a crucial role in facilitating their reproductive success and enabling them to thrive in marine, freshwater, and terrestrial environments throughout their evolutionary history of over 500 million years (Mann, 1988). Shell composition is dynamically changing during shell morphogenesis, especially in polymorphic calcium carbonate (CaCO₃) crystals and structurally modified shell layers (Rose and Baker, 1994). During early shell formation, the shells of bivalve larvae have been divided into prodissoconch I (PI), which consists mainly of amorphous calcium carbonate (ACC), and prodissoconch II (Zhao et al., 2018; Lee et al., 2006;

Aranda-Burgos et al., 2014; Miyazaki et al., 2010). ACC distinguishes early shells from the calcite and aragonite found in adult shells (Marin, 2012; Moueza et al., 2006). Molluscan adult shells consist of an organic-mineral complex in which 1–5 % of the organic matrix component provides the framework for 95 % of the mineral deposits (Addadi et al., 2006; Suzuki et al., 2009). In particular, the organic matrix includes glycoproteins, chitin, and acidic polysaccharides, which serve as the primary regulators of the nucleation and growth of CaCO₃ crystals (Nudelman et al., 2006). Of these, the concept of an “initial non-calcified shell” (InCaS) has been proposed, which contains only an organic matrix that resembles the periostracum of adult shells and is distinct from the calcified shell formation (Huan et al., 2013). However, the molecular

Abbreviations: ACC, Amorphous Calcium Carbonate; BMP, Bone Morphogenetic Protein; CaCO₃, Calcium Carbonate; *CgTyrp-2*, Tyrosinase-like Protein 2; *CgTyr*, Tyrosinase; *CgChit4*, Chitinase; *CgChs1*, Chitin Synthase; *C. gigas*, *Crassostrea gigas*; DMSO, Dimethyl Sulfoxide; EF1- α , Elongation factor 1- α ; InCaS, Initial non-Calcified Shell; MFSW, Millipore-Filtered Sea Water; NJ, Neighbor-Joining; OTs, Off-Target Sites; PI, Prodissoconch I; PTU, Propylthiouracil; PFA, Paraformaldehyde; PBS, Phosphate Buffer Solution; SMPs, Shell Matrix Proteins; SEM, Scanning Electron Microscope; RT-qPCR, Reverse Transcription Quantitative PCR; RS18, Ribosomal protein S18.

* Corresponding author at: Key Laboratory of Mariculture, Ministry of Education, Ocean University of China, Qingdao 266003, China.

E-mail address: qili66@ouc.edu.cn (Q. Li).

<https://doi.org/10.1016/j.gene.2024.148748>

Received 8 May 2024; Received in revised form 11 June 2024; Accepted 2 July 2024

Available online 3 July 2024

0378-1119/© 2024 Elsevier B.V. All rights are reserved, including those for text and data mining, AI training, and similar technologies.

mechanisms of InCaS formation in oysters remain unknown. Simultaneously, a comprehensive understanding of the PI shell formation process is important to understand how the molluscan shell emerged during evolution.

In recent years, bioinformatics-omics methodologies have been widely applied to uncover the molecular mechanisms connected to the development of shells in different bivalves, including oysters, clams, and mussels (Feng et al., 2017; Liao et al., 2015; Arivalagan et al., 2017; Feng et al., 2015). A comparative proteomic analysis of the Pacific oyster (*Crassostrea gigas*) reveals marked differences in shell matrix proteins (SMPs) between adults and larvae, but share some functional domains, such as von Willebrand factor type A, chitin binding, and carbonic anhydrase, emphasizing the role of calcification in early shell formation (Song et al., 2019). Furthermore, the molecular mechanism of shell formation involves multiple levels and is governed by a complex network of genes, including tyrosinase, chitinase, chitin synthase, and bone morphogenetic protein (BMP) (Luo et al., 2015; De Wit et al., 2018; Ramesh et al., 2019). While tyrosinase genes are known for their involvement in molluscan shell pigmentation, their potential roles in early shell formation cannot be disregarded (Zhu et al., 2021; Yang et al., 2017).

Tyrosinase (EC 1.14.18.1) is a type three copper protein, which is characterized by two copper-binding domains in its sequence (Chang, 2009). Their function in mollusks' initial shell formation, regeneration, and melanin synthesis has been well explored (Zaidi et al., 2016; Liu et al., 2019; Zhu et al., 2022; Chen et al., 2017; Jiang et al., 2020; Feng et al., 2019; Miglioli et al., 2019). *HcTyr* and *Hctyp1* were shown to be involved in the deposition of the color of the pearl layer of *Hyriopsis cumingii* and *RpTyr9* was engaged in the formation of the shells and color of *Ruditapes philippinarum* (Chen et al., 2017; Jiang et al., 2020). Recently, the knockdown of a tyrosinase gene by dsRNA interference using algal commensalism blocked adult shell growth and color formation in *C. gigas*, suggesting that tyrosinases play important roles in the assembly and maturation of the shell structures (Feng et al., 2019). Similarly, in the early larval stages of *Mytilus galloprovincialis*, significant growth deformities and impaired shell calcification are observed upon the use of propylthiouracil (PTU), a well-known inhibitor of tyrosinase synthesis (Miglioli et al., 2019). The tyrosinase family underwent genetic expansion during the evolution of *C. gigas* (Aguilera et al., 2014; Huang et al., 2017). However, investigations into the tyrosinase genes of *C. gigas* have been limited to clonal expression and sequence analysis. In the localization of *CgTyrp-2* in *C. gigas* larvae had been hypothesized to be involved in early shell formation, but these efforts have largely resulted in speculative hypotheses (Huan et al., 2013). In the last decade, the CRISPR/Cas9 system has emerged as a highly promising and versatile tool for studying gene function. Its efficacy has been demonstrated in various model and non-model species, such as mice, zebrafish, Atlantic salmon, sea urchins, and *Ciona* (Bai et al., 2016; Ablain et al., 2015; Edvardsen et al., 2014; Edgar et al., 2019; Gandhi et al., 2017). Li et al. and Huan et al. had utilized CRISPR/Cas9 technology to validate *CgSmhc* in oyster muscle formation and *LgCalaxin* in cilia formation in gastropods, respectively, and detect corresponding phenotypic changes (Li et al., 2021; Huan et al., 2021).

In this study, we monitored the deposition process of organic substrate and calcified shell during the early shell formation in *C. gigas* utilizing calcofluor and calcein staining. In addition, based on sequence comparisons, homology analysis, and exploration of tyrosinase gene expression across various periods of the larval transcriptome in *C. gigas*, we identified and focused on two tyrosinase genes (*CgTyr* and *CgTyrp-2*) and their expression was verified by RT-qPCR. Finally, CRISPR/Cas9 technology was utilized to confirm that the *CgTyr* and *CgTyrp-2* were involved in the calcium carbonate deposition process in the early shells of *C. gigas*. These results will improve our understanding of the initial shell formation process in mollusks and lay the foundation for understanding the molecular mechanisms of shell growth and development.

2. Materials and methods

2.1. Preparation of fertilization and rearing of *C. gigas*

The adult *C. gigas* were sourced from a local oyster farm in Rongcheng, China. Six adult tissues (edge mantle, central mantle, adductor, gills, labial palp, and digestive gland) were first taken and three biological replicates were in place. Additionally, mature female and male oysters were selected, and in vitro fertilization was previously described (Li et al., 2021). Subsequently, embryo and larval samples were obtained according to previously reported procedures (Min et al., 2022), including the specific sampling times (Table S1).

These samples were flash-frozen at liquid nitrogen and stored at -80°C freezer until RNA isolation.

2.2. Larval development and shell biogenesis

Shell biogenesis was followed at different hours post-fertilization (8, 10, 12, 18 and 24 hpf), by evaluating the growth of both the organic matrix and calcified shell components using fluorescent dyes (Miglioli et al., 2019). Calcein (Sigma Aldrich) was added to the culture medium (final concentration 1 mM in 0.01 % DMSO) before the addition of fertilized eggs. Calcofluor white Fluorescent Brightener 28 (Sigma-Aldrich) was directly added to the single wells on live larvae five minutes before each sampling time (final concentration 0.02 mM in 0.01 % DMSO). At each sampling time, the larvae were washed three times with millipore-filtered sea water (MFSW) to remove excess dyes and then fixed with 4 % paraformaldehyde (PFA). The samples were immediately imaged using a Leica TCS SP8 (Leica). Calcofluor (UV channel, Exc: 408 nm/Em: 450–490 nm) gave a blue signal for the organic matrix, while calcein (FITC channel, Exc: 488 nm/Em: 520–560 nm) visualized the calcified shell in green.

A scanning electron microscope (SEM) was performed to examine larval shell morphogenesis. Briefly, samples were fixed in 2.5 % glutaraldehyde in 0.1 M phosphate buffer solution (PBS) and then refixed in 1 % osmic acid. After fixation, samples were washed in PBS and dehydrated using graduated ethanol. Subsequently, samples were dehydrated with chloroform. Once dried, samples were coated with gold and scanned with a VEGA3 TESCAN scanning electron microscope.

2.3. Sequence and phylogenetic analysis

The amino acid sequences of tyrosinase and tyrosinase-like proteins from *Danio rerio*, *Mus musculus*, *Pinctada fuata*, *Petromyzon marinus*, *Hyriopsis cumingii*, *Mytilus corucus*, *M. galloprovincialis*, *Crassostrea angulata*, and *C. gigas* were retrieved from the NCBI database followed by further manual curation and phylogenetic analysis. The functional domains were predicted using SMART software (<https://smart.embl-heidelberg.de/>). Sequence alignment of the domains was performed using the DNAMAN version 8.0 (Lynnon BioSoft, USA). Signal 4.1 program (<https://www.cbs.dtu.dk/services/SignalP/>) was used to predict the signal peptide of tyrosinase or tyrosinase-like protein. The hit sequence was subsequently submitted to phylogenetic analysis using the Neighbor-Joining (NJ) method (MEGA X package, <https://megasoftware.net/>). Whole amino acids were used, and 1000 bootstrap replicates were calculated in the phylogenetic analysis.

2.4. cDNA synthesis and RNA expression analysis of *CgTyr* by real-time quantitative PCR

Total RNA of samples from different adult tissues and different embryo-larval development stages were extracted with Trizol® reagent (Thermo Fisher Scientific) according to the manufacturers' instructions. The total RNA was reverse transcribed into cDNA by PrimeScript™ Reverse Transcription Kit (Takara). So only the transcript levels of *CgTyr* in embryo-larval developmental stages and different adult tissues were

quantified by RT-qPCR. The RT-qPCR was amplified using SYBR®Premix ExTaq™ II kit (Takara) on a LightCycler®480 real-time PCR system (Roche) according to the manufacturer's protocols. The specified primers were designed (Table 1), and their specificity was detected by conventional PCR and melting curve analyses. Elongation factor 1- α (EF1- α) and ribosomal protein S18 (RS18) were the internal control primers in the adult and embryo-larval samples, respectively (Du et al., 2013; Sun et al., 2023). The relative expression was calculated by the 2^{- $\Delta\Delta$ CT} method. All data and the significant differences were analyzed using the IBM SPSS Statistics 22 by one-way ANOVA followed by multiple comparisons. Differences were considered statistically significant at $P < 0.05$.

2.5. Preparation of sgRNA and Cas9mRNA

Three exons of *CgTyrp-2* and *CgTyr* were selected for CRISPR-induced mutagenesis. The target sites were predicted using an online tool CRISPOR (<https://crispor.tefor.net/>). Five sgRNAs of *CgTyrp-2* were designed and named *CgTyrp-2*-sgRNA-38, *CgTyrp-2*-sgRNA-64, *CgTyrp-2*-sgRNA-12, *CgTyrp-2*-sgRNA-54, *CgTyrp-2*-sgRNA-116, respectively. Three sgRNAs of *CgTyr* were designed and named *CgTyr*-sgRNA-222, *CgTyr*-sgRNA-261, and *CgTyr*-sgRNA-331, respectively. The synthesizing *CgTyrp-2*-sgRNAs and *CgTyr*-sgRNAs were referenced to the previous methods (Li et al., 2021). The primers were provided (Table 1, Table S2). Furthermore, the pT3TS-nCas9n plasmid was linearized by XbaI (NEB) and purified by a MiniElute PCR Purification Kit (Qiagen). The linearized plasmid was used as the template for in vitro transcription to generate capped Cas9mRNA using the T3 RNA polymerase kit (Ambion,

America). The synthesized Cas9mRNA and sgRNAs were purified and extracted using phenol–chloroform.

2.6. Microinjection of *C. gigas* embryos

The Cas9 mRNA and sgRNAs were diluted with Cas9 working buffer (0.5 % phenol red, 20 mM HEPES and 150 mM KCl) at 500 ng/ μ l, and delivered into fertilized *C. gigas* eggs by microinjection. Approximately 0.1 nL of sgRNA/Cas9 solution was injected into the one-cell stage *C. gigas* embryo. And a blank control and a negative control with only cas9 mRNA were in place (Table 2, Table S3). Microinjection was carried out by using a Warner PLI-100A Pico-Injector microinjector (Warner Instruments). Embryos were injected under an inverted microscope IX73 (Olympus) by using two micromanipulators for holding and microinjection pipettes (Narishige). The injected embryos in each group were counted in Table 2 and Table S3.

2.7. Larval DNA extract and indels detection by sanger sequencing

The genomic DNA was extracted from D-veliger larvae using the Chelex®-100 method (Li et al., 2021). The genomic region flanking the target site was amplified with 2 \times Taq Plus Master Mix II (Dye Plus) (Vazyme) according to the manufacturer's instructions. Sanger sequencing of PCR products was shown using the CRISPR Edits (ICE) online tool (Conant et al., 2022). The PCR fragments were purified and then cloned into a pMD19-T vector (Takara). Twelve clones were randomly selected for DNA sequencing using M13 primers. Similarly, Mali et al. (Ventura et al., 2016) reported that Cas9/sgRNA binding

Table 1
Primers for sgRNA synthesis, PCR analyses, and RT-qPCR validation.

Primer name	Gene ID	Sequence (5'-3')	Primer's intro/ exon location	uses
<i>CgTyrp-2</i> -sgRNA-64-F	105,344,040	GATCACTAATACGACTCACTATAG GTGCGGGCTCGGTGATTGGG TTTTAGAGCTAGAAAT	5'UTR	sgRNA synthesis
<i>CgTyrp-2</i> -sgRNA-12-F	105,344,040	GATCACTAATACGACTCACTATAG GGAAGGCATGGGTACCCGAC TTTTAGAGCTAGAAAT	Exon3	
<i>CgTyrp-2</i> -sgRNA-54-F	105,344,040	GATCACTAATACGACTCACTATAG GGGCCITGCTGTCCAGGAGAG TTTTAGAGCTAGAAAT	Exon4	
<i>CgTyr</i> -sgRNA-261-F	105,329,903	GATCACTAATACGACTCACTATAG GGGGGCAACCGTCCAATACAG TTTTAGAGCTAGAAAT	Exon1	
sgRNA-reverse	–	AAAAGCACCGACTCGGTGCC	–	
RT- <i>CgTyrp-2</i> -F	105,344,040	TCAGAAACGAGGAAAAAGACAA	Exon1	RT-qPCR specific primer
RT- <i>CgTyrp-2</i> -R		GGAGTGAAGCGAGGCGAT	Exon2	
RT- <i>CgTyr</i> -F	105,329,903	GGGCAACCGTCCAATACAC	Exon1	
RT- <i>CgTyr</i> -R		GTGCTATTGGACTCCCTTC	Exon2	
RT- <i>CgChit4</i> -F	105,331,570	ATTGGAGCCTCAGCCGTG	Exon8	
RT- <i>CgChit4</i> -R		TGTCGTCGTAACCAACCCA	Exon9	
RT- <i>CgChs1</i> -F	105,324,613	AAGCCTCACACTTTACCAGAA	Exon12	
RT- <i>CgChs1</i> -R		TTGATACCAGACAATCGGACC	Exon13	
RT-EF1 α -F	105,338,957	CCATTGAGAGGAAAGAGGGAA	Exon6	RT-qPCR internal control primer
RT-EF1 α -R		CCAACCTGGCACTGTCCAATAC	Exon7	
RT-RS18-F	105,347,800	CGTGAGGATCTGGAGCGA	Exon4	
RT-RS18-R		TTTTCTCCCTCATTACACA	Exon5	
TB- <i>CgTyrp-2</i> -F1	105,344,040	TCAAATACGAGACGTGAATCCATG	Intro1	SNP validation for <i>CgTyrp-2</i> -sgRNA-64/38/116
TB- <i>CgTyrp-2</i> -R1		TAACGCACCTTGGATTCTTGATTG	5'UTR	
TB- <i>CgTyrp-2</i> -F2	105,344,040	GGTTTATCTCCTGGTGTAAGTCT	Exon2	SNP validation for <i>CgTyrp-2</i> -sgRNA-12
TB- <i>CgTyrp-2</i> -R2		ATCTTCAAAGGGTCCAGTCAG	Exon3	
TB- <i>CgTyrp-2</i> -F3	105,344,040	ATGCCTTACTGGGACATGACTA	Exon3	SNP validation for <i>CgTyrp-2</i> -sgRNA-54
TB- <i>CgTyrp-2</i> -R3		GAACCTCGAAGTCTCTTGGGTA	Exon4	
TB- <i>CgTyr</i> -F1	105,329,903	TGATAGAAAACCTGGAATACCC	Exon1	SNP validation for <i>CgTyr</i> -sgRNA-261/331
TB- <i>CgTyr</i> -R1		GTTGTGCATGAGGTTTAAACAAT	Exon1	
Ld- <i>CgTyrp-2</i> -F	105,344,040	TTGTTTTCCAGGGCAATTAC	5'UTR	<i>CgTyrp-2</i> large deletion
Ld- <i>CgTyrp-2</i> -R		GGGTCCCAAGAAGCTGTGTTA	Exon4	

Note: The bold sequences in *CgTyrp-2*-sgRNAs and *CgTyr*-sgRNAs were the gene-specific target sequences within the respective sgRNAs. The bold parts in sgRNAs were added by PCR primer for correct T7 transcription.

could tolerate up to three mismatches. The possible off-target sites of sgRNAs were predicted using the online tool (<https://crispor.tefor.net/>). The off-target loci were amplified with the primers in Table S2 by PCR and identified by sequencing.

2.8. Expression analysis of related genes after *CgTyrp-2* or *CgTyr* knockout

RT-qPCR was used to investigate the effect of the knockout at the mRNA levels. The larval total RNA was extracted using MicroElute Total RNA Kit (Omega) according to the manufacturers' instructions (15 larvae as a group and three biological replicates). The total RNA was reverse transcribed into cDNA by HiScript III 1st Strand cDNA Synthesis

Kit (Vazyme). The qPCR was amplified using ChamQ SYBR Color qPCR Master Mix (Vazyme) on a LightCycler®480 real-time PCR system (Roche) according to the manufacturer's protocols. The specific primers and internal control primers were shown in Table 1. Calculation of the relative expression was utilizing the $2^{-\Delta\Delta CT}$ method. All data and the significant differences were analyzed using the IBM SPSS Statistics 22. Differences were considered statistically significant at $P < 0.05$.

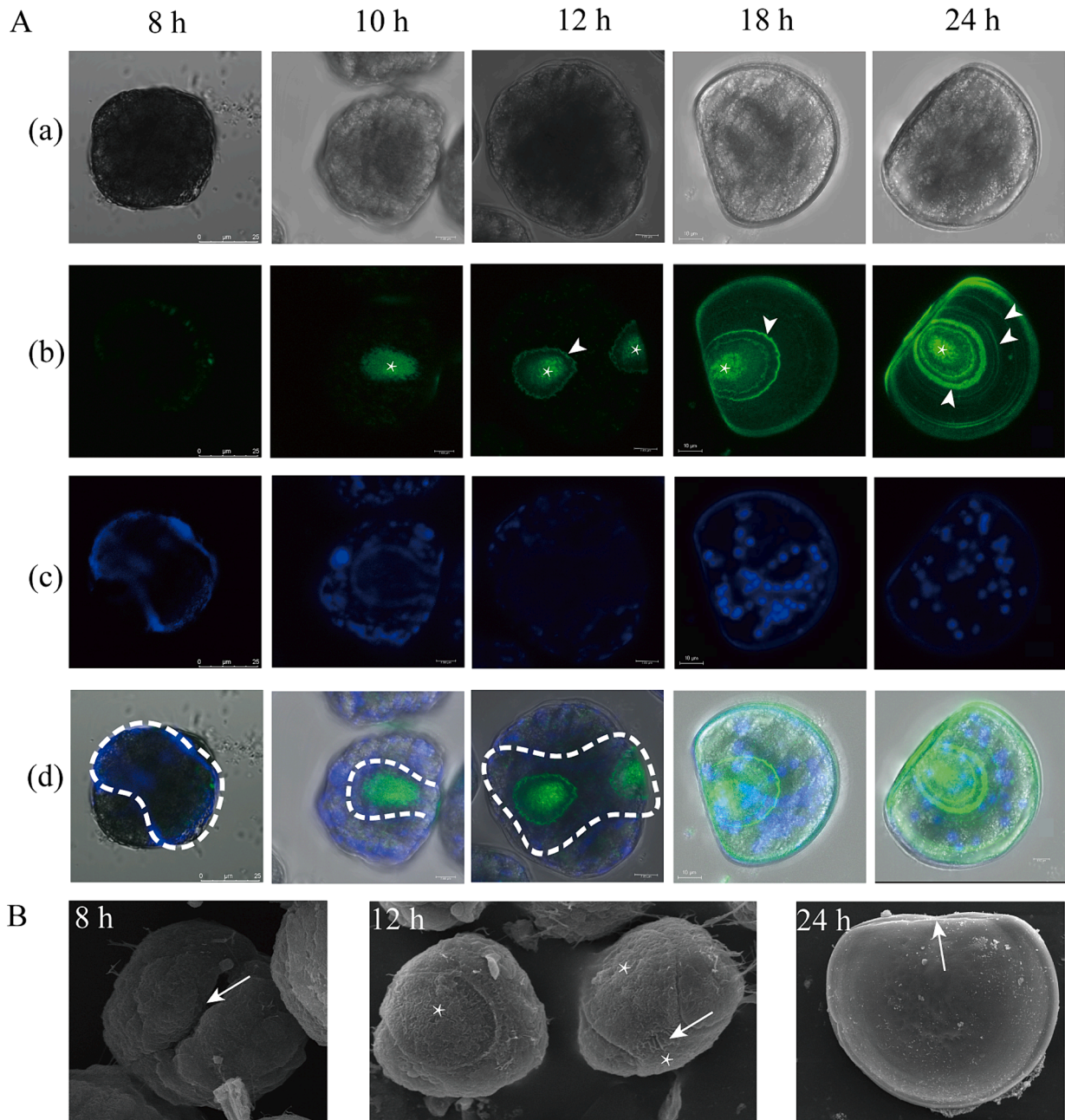


Fig. 1. Identify key periods of shell formation. A: Confocal images showing the time course of shell formation in *C. gigas* from gastrula (8 hpf) to the D-veliger stage (24 hpf). (a) Brightfield image of the embryo; (b) calcein fluorescence signal (green and asterisk); (c) calcofluor fluorescent signal (blue); (d) merged calcofluor, calcein, and brightfield images. The arrowheads pointed to the access rings. B: SEM analysis of larval development in *C. gigas*. At 8 hpf, the shell-gland began to be seen as a slit (arrow). At 12 hpf, the shell-field was visible as a bilateral ribbon (asterisk). The arrows pointed to the hinge area. At 24 h, the shell-field further expanded to cover the entire larvae. The straight hinge line was indicated by the arrow.

3. Results

3.1. Identification of the key periods for organic production and calcium deposition during early shell formation in *C. gigas*

The double calcofluor/calcein staining was employed to investigate the distribution of organic matrix and the deposition of CaCO_3 during the early development in *C. gigas*. At 8 hpf, the organic matrix was secreted in the gastrula larvae, and the calcofluor signals (blue) were mainly visible in a saddle-shaped area, but calcein staining was not observed, indicating the absence of stable CaCO_3 deposition (Fig. 1A). The Larvae started swimming in situ under the rotating of cilia at 8 hpf, and deep depression (arrow) appeared dorsally (Fig. 1B). At 10 hpf, the calcification signals (green) were observed in the center of the forming valve (asterisk) and the subshell of the rugose extended from dorsal to ventral (Fig. 1A). At 12 hpf, the larval shell showed the shape characteristic of the early veliger stage: the middle shell-field (arrow) would become the hinge and completely flattened (Fig. 1B). In addition, the valves are heavily calcified, indicating the gradual deposition of CaCO_3 to form the calcium ring (arrowhead) (Fig. 1A). The calcified shell covered the organic matrix, except for a thin layer along the margins of the valve. At 18–24 hpf, the embryo developed to the D-veliger stage, where the calcified shell covered the whole body of the larvae, and showed more evident concentric accretion rings (arrowheads) (Fig. 1A).

3.2. Phylogenetic analyses of tyrosinase genes in *C. gigas* and their high expression in shell-field periods

Two tyrosinase genes *CgTyr* (LOC105329903) and *CgTyrp-2* (LOC105344040) were identified in *C. gigas*. Amino acid sequence alignments of *CgTyr* and *CgTyrp-2* genes from *C. gigas* and other bivalves were performed. The signal peptide revealed that *CgTyr* and *CgTyrp-2* possessed a transmembrane region in addition to a conserved Cu(A)/Cu(B) domain (Fig. 2A). Amino acid sequence comparison revealed a conserved copper-binding domain Cu(A) and Cu(B), in which six histidine residues were highly conserved (Fig. 2B). The different species of phylogenetic tree analysis were carried out to indicate the evolutionary relationships of tyrosinases. *CgTyrp-2* was close to the tyrosinase of *C. angulata* with 100 % similarity, which belongs to the same clade. *CgTyr* shared the highest identity with tyrosinase-like protein 3 of *M. galloprovincialis* and *H. cumingii* (Fig. 2C). All tyrosinases of mollusk were grouped into a close cluster. The tyrosinases from *D. rerio* and *M. musculus* were classified as a vertebrate clade.

The expression patterns in embryonic and larval stages were analyzed. The results showed that *CgTyr* was mainly expressed in the trochophore and early D-veliger stages, with particularly high expression in the early D-veliger larvae (Fig. S1A). This is consistent with the timing of the onset of calcification in the shell-field of *C. gigas*. The expression patterns of *CgTyr* in various tissues were also analyzed. The results revealed that high expression levels of *CgTyr* mRNA were detected in the mantle, especially at the edge of the mantle (Fig. S1B).

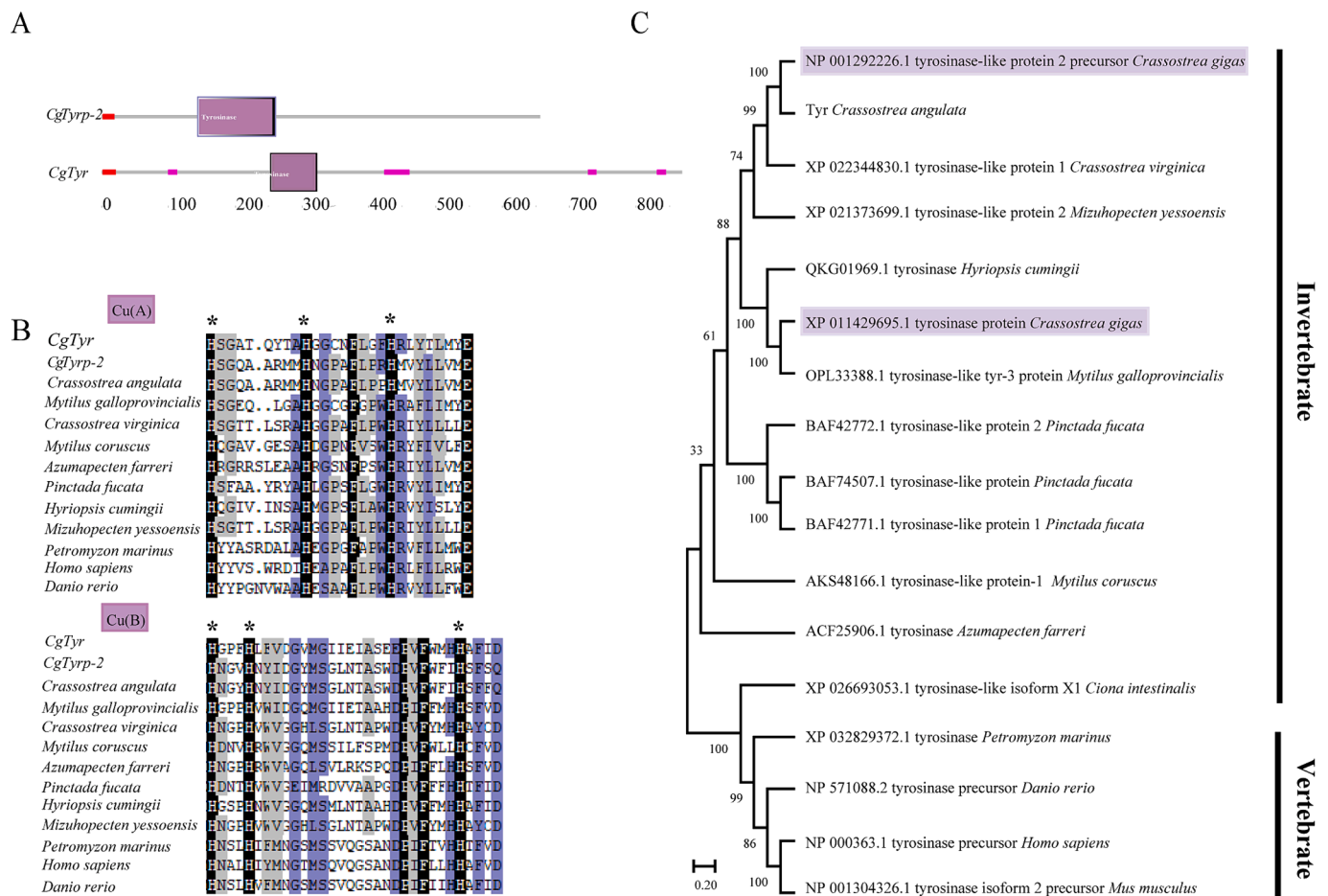


Fig. 2. A schematic of *CgTyr* and *CgTyrp-2*. A: The signal peptide was located at the N-terminus, followed by two copper-binding domains Cu(A) and Cu(B) comprising the catalytic center. The conserved histidine residues were highlighted in red, and pink boxes indicate low-complexity regions. B: Multiple alignment of the two copper-binding domains Cu(A) and Cu(B) between *CgTyr* and *CgTyrp-2* genes. The six conserved histidine residues were indicated by asterisks. C: Phylogenetic analysis of the tyrosinases.

3.3. Identification of effective sgRNAs and testing of mutation efficiency

CRISPR/Cas9 was employed to further tyrosinase gene function during early shell formation in *C. gigas*. Firstly, five sgRNAs and three sgRNAs for exons were designed at different positions of *CgTyrp-2* and *CgTyr* (Fig. 3A), respectively, and the different sgRNAs showed different mutation efficiency (Table S3). According to the sequencing results, *CgTyrp-2*-sgRNA-64 injection, *CgTyrp-2*-sgRNA-12 injection, *CgTyrp-2*-sgRNA-54 injection, and *CgTyr*-sgRNA-261 injection showed obvious multiple peaks near the protospacer adjacent motif (PAM) sites of the

target sites (Fig. 3B), which would be used to carry out subsequent experiments. Injection of other sgRNAs did not cause detectable effects on the target sites, suggesting that the efficiency was introduced with low efficiency (Fig. S2). The targets induced with the *CgTyrp-2*-sgRNA-12 injection, *CgTyrp-2*-sgRNA-54 injection, and *CgTyr*-sgRNA-261 injection were mainly small indel mutations with sizes of 1–21 bp, 1–10 bp and 1–9 bp (Fig. S3). The types of indent mutations at the three target sites were mainly insertions and deletions that may alter the translation of proteins and disrupt the function of genes.

CgTyrp-2-sgRNA-64 and *CgTyrp-2*-sgRNA-54 were comparable in

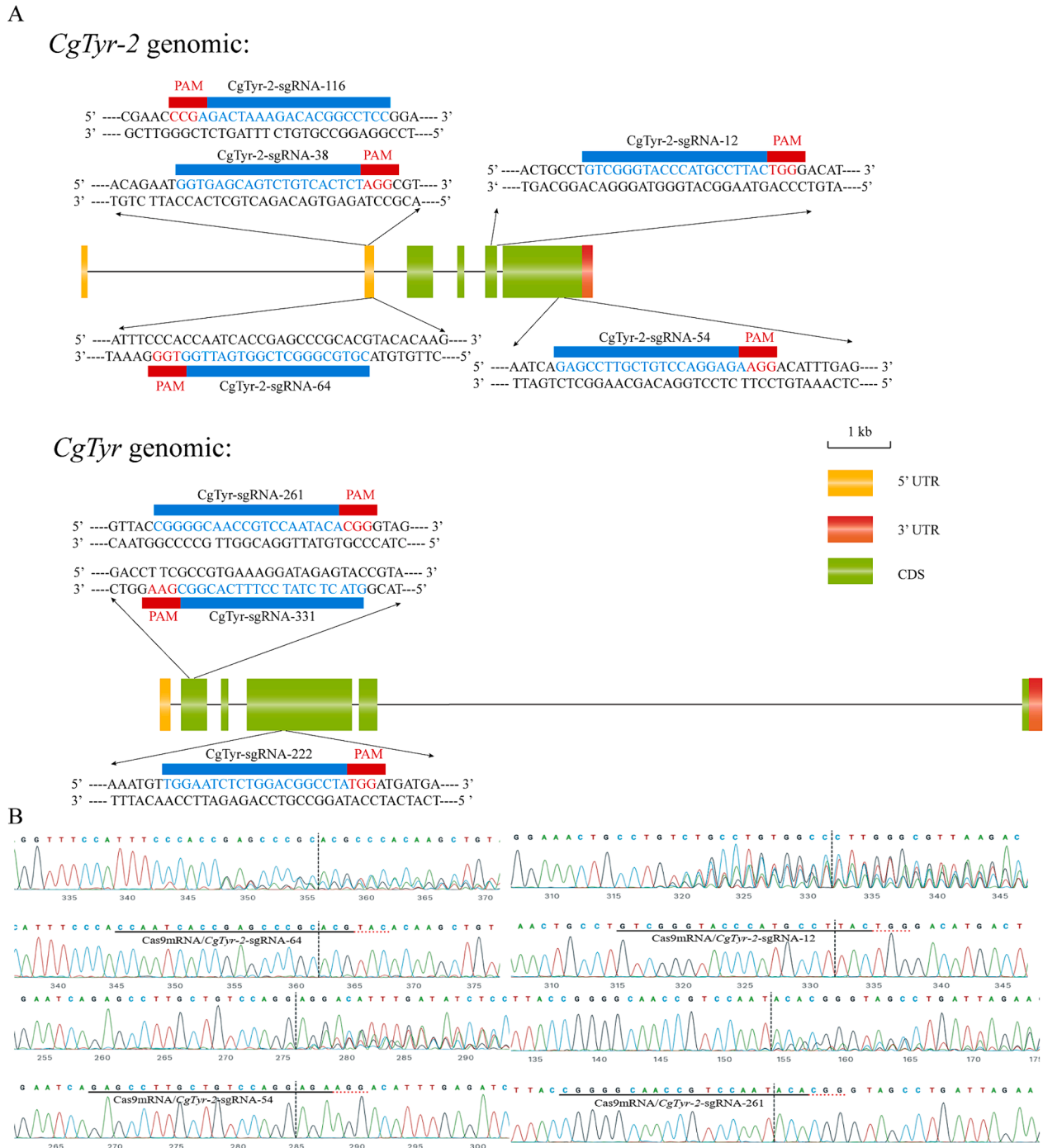


Fig. 3. Schematic diagram of *CgTyr*-sgRNAs and *CgTyrp-2*-sgRNAs. A: The PAMs were shown in red, and the sgRNA sequences were shown in blue. sgRNA-64 was located at 5'UTR of *CgTyrp-2*; sgRNA-12/54 were located at the penultimate two exons of *CgTyrp-2*; sgRNA-261 was located at second exon of *CgTyr*. **B:** Sanger sequencing of PCR products was shown using the CRISPR Edits (ICE) online tool (<https://www.ice.synthego.com>) and indel mutations in injected embryos were characterized. The *CgTyrp-2*-sgRNA-64/12/54 and *CgTyr*-sgRNA-261 injected embryos showed evident multiple peaks near the PAM sites of the target sequences.

efficiency, *CgTyrp-2*-sgRNA-12 was the most efficient but still could not achieve 100 % knockout rate (Table 2; Table S3). *CgTyrp-2*-sgRNA-64 and *CgTyrp-2*-sgRNA-12, crossing three exons, were mixed in equal concentrations and injected into one-cell stage embryos. Furthermore, a large fragment deletion (2 kb) was observed within the *CgTyrp-2* gene (Fig. S4).

3.4. Expression of related genes after knockout of *CgTyrp-2* or *CgTyr*

It was shown that chitin proved to be a key component of the shell matrix, and the expression of chitinase (*CgChit4*) and chitin synthase (*CgChs1*) were indeed correlated with the formation of the larval shell. Subsequently, to assess the effect of knockout at the mRNA levels, the expression of *CgTyrp-2*, *CgTyr*, *CgChs1* and *CgChit4* was quantified by RT-qPCR. The results showed that the expression of *CgTyrp-2* was severely down-regulated in larvae injected with *CgTyrp-2*-sgRNA-64/54 (Fig. 4A). Moreover, knockout of *CgTyrp-2* resulted in a significant up-regulation of *CgChit4* and *CgTyr* expression and a significant down-regulation of *CgChs1* in larvae (Fig. 4). In the larvae injected with *CgTyr*-sgRNA-261, the expression of *CgTyr* was severely down-regulated (Fig. 4B). In addition, *CgTyr* knockout resulted in a significant upregulation of *CgChit4* expression and a significant downregulation of *CgChs1* in larvae (Fig. 4). Interestingly, there was no genetic compensation effect of *CgTyrp-2* and *CgTyr* with each other after knockout by single gene (*CgTyr*) (Fig. 4).

3.5. Effect of knockout tyrosinases on early shell development

The early development of *C. gigas* after injection of the Cas9-sgRNA complex was consistent with that of control larvae. Early cleavage was unaffected, and there were no obvious phenotypic differences in the larvae under ordinary light microscopy. To further investigate whether differences in shell developmental microcomponents occurred, the larval shell was stained by the above dichroic method. *CgTyrp-2* or *CgTyr* were knocked out for 24 hpf, and the larvae successfully developed into D-veliger. However, deposition and growth of shell substrate was delayed and the shells formed a distinctly asymmetrical calcified (Fig. 5).

To explore whether the tyrosinase genes had a genetic compensation in shell formation. After *CgTyrp-2* and *CgTyr* were co-knocked out together for 24 hpf, we further observed heterogeneity in the calcification patterns with dichroic staining, and the shells did not show the typical hyperplastic ring (arrows) (Fig. 5). Various strong shell surface aberrations were evident compared to control samples: irregular calcification patterns, valves with asymmetric growth of organic matrix and calcification. Furthermore, shell changes in knockout larvae were reflected in a significant reduction in the area of the shell matrix and

Table 2

Summary of gene targeting efficiency, incubation rate and phenotype rate.

	survival D-veliger larvae/No. of embryos injected	Target points mutation/sequenced larvae	Phenotypic mutation rates
Uninjected control	70/115	0/5	–
Cas9 mRNA injection	46/130	0/5	–
<i>CgTyrp-2</i> -sgRNA-12 injection	36/98	14/15	–
<i>CgTyrp-2</i> -sgRNA-261 injection	50/200	8/10	3/15
<i>CgTyrp-2</i> -sgRNA-64/54 injection	47/132	12/12	4/15
<i>CgTyrp-2</i> -sgRNA-12/ <i>CgTyr</i> -sgRNA261 injection	56/169	–	5/10

Note: The short horizontal line indicates no statistics.

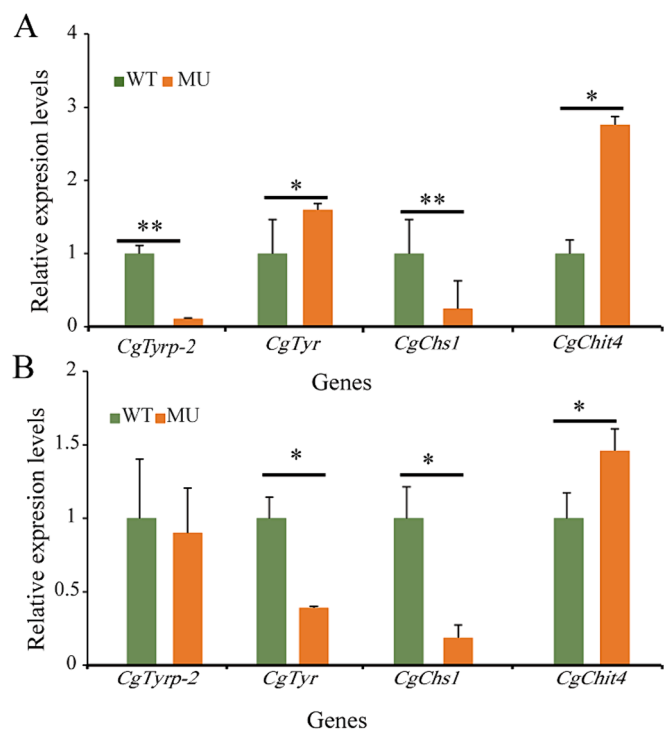


Fig. 4. Knockout effect of *CgTyr* or *CgTyrp-2* on the RNA level. A: The expression of *CgTyrp-2* and *CgChs1* were severely down-regulated in larvae with Cas9mRNA/*CgTyrp-2*-sgRNA-64/54 injection, but the expression of *CgChit4* and *CgTyr* were up-regulated in larvae. B: The expression of *CgTyr* and *CgChs1* were severely down-regulated in larvae with Cas9mRNA/*CgTyr*-sgRNA-261 injection, but the expression of *CgChit4* was up-regulated in larvae. The larvae in the figures were at the early D-veliger stage (18 hpf). *, P < 0.05; **, P < 0.01.

calcified shell. In addition, the deletion of *CgTyrp-2* and *CgTyr* did not result in changes in larval hatching rates (Table S3). We could not determine whether these larvae could metamorphose since metamorphosis of *C. gigas* could not occur under the current culture system in the lab. In an occasional case, the larvae were cultured for a week, and we did not observe decreases in viability.

3.6. Off-target validation

To verify whether multiple sgRNAs can cause any off-targeting effects, we examined five off-target sites (OTs) in total (Table S4). Sequencing analysis of potential OTs in mutant oysters showed an absence of mutations in OTs, indicating no off-target effects within the assay range (Fig. S5). All these indel mutations were frameshift mutations that alter the protein translation and disrupt the gene function.

4. Discussion

4.1. The dynamic patterns of shell formation in *C. gigas* during early development

The process of initial shell formation commenced early in embryonic development, with shell-field originating from ectodermal cells (Ventura et al., 2016). Before shell calcification, the shell-field results in the secretion of organic matrix by ectodermal cells through invagination and evagination. We confirmed a significant time interval between the secretion of organic matrix and the deposition of CaCO₃ during the early developmental stages of the oyster by simultaneous double staining with calcofluor white Fluorescent-labeled organic matrix and calcein-labeled CaCO₃ (Kurita et al., 2009). The early secretion of the organic matrix would protect the initial shell against dissolution, particularly in acidic

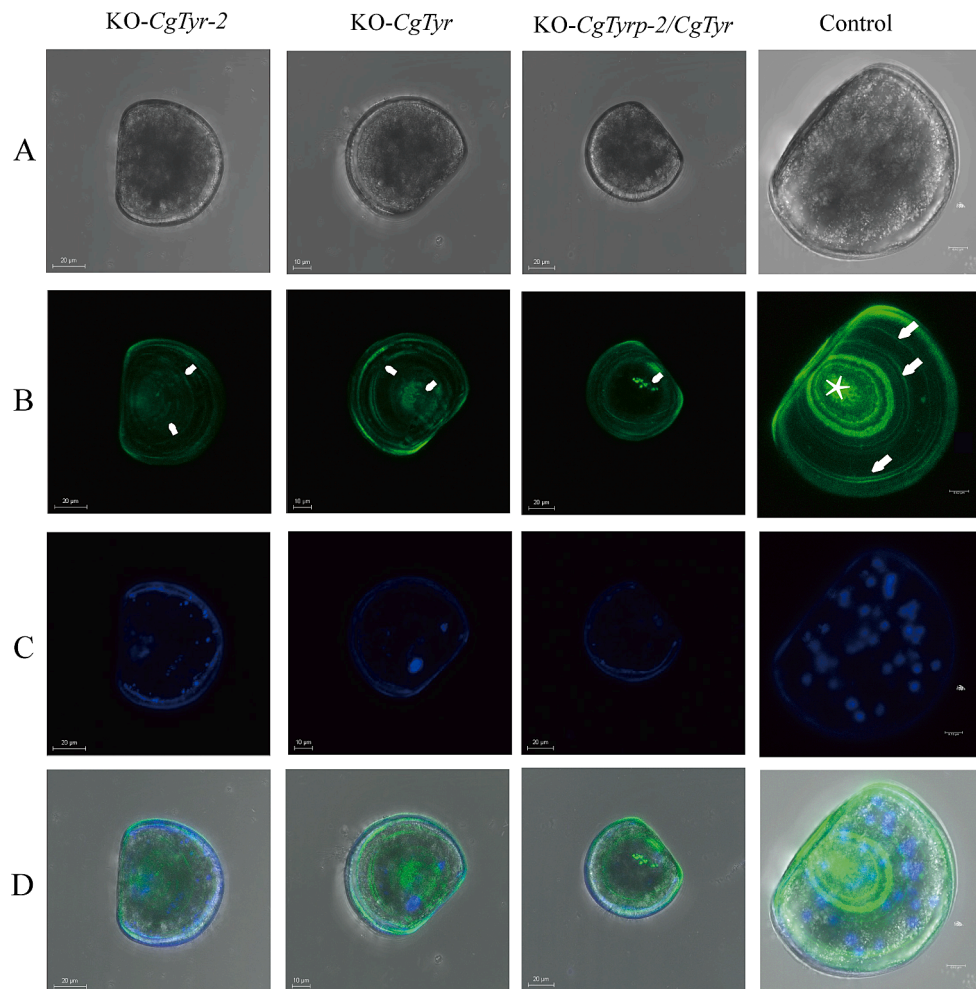


Fig. 5. Shell of D-veliger larvae after *CgTyrp-2* and *CgTyr* deletion The effect of tyrosinase deficiency on early shell formation in *C. gigas*. In particular, the 24 h sample in Fig. 1A will be used as a control. A, Brightfield image of the embryo; B, calcein fluorescence signal (green); C calcofluor fluorescent signal (blue); D, merged calcofluor, calcein, and brightfield images. KO indicated knockout. The calcified shell and rings were pointed by arrow and asterisk.

mangrove environments (Yang et al., 2020). Furthermore, the expansion of the shell-field with larval development was always accompanied by the secretion of organic matrix and deposition of CaCO_3 . The PI shell added the calcium ring from the central shell-field outward, which had been ignored in previous descriptions. Our results demonstrate the close interaction between the organic matrix of the shell layer and calcification.

4.2. The expression patterns of *CgTyr* and *CgTyrp-2* in different tissues, embryonic and larval stages

During the adult stage, *CgTyr* and *CgTyrp-2* were predominantly expressed in the mantle of *C. gigas*. In bivalves, tyrosinase genes were highly expressed in the mantle, which was responsible for biomineralization or pigmentation (Nagai et al., 2007; Yao et al., 2020; Ren et al., 2020). The mantle was divided into two regions in bivalves, namely, the marginal mantle involved in the mineralization of prismatic layers, and the central mantle associated with the formation of nacre layers (Zaidi et al., 2016). Expression of *CgTyr* and *CgTyrp-2* genes was mainly observed in the marginal mantle, and less in the central mantle, suggesting that they were associated with the formation of prismatic shell layers or periostracal structures.

During embryo-larval development, *CgTyrp-2* and *CgTyr* mRNA were mainly expressed at the trochophore and early D-veliger (18 hpf) stages. The expression patterns of *CgTyrp-2* and *CgTyr* were consistent with those of the tyrosinase genes of the bivalves *Meretrix meretrix* and

H. cumingii (Yao et al., 2020; Ren et al., 2020). Furthermore, based on the expression patterns of *CgTyr* and *CgTyrp-2* in *C. gigas* adults and larvae, it coincided with the previous observation that shell-field first appeared at the end of the gastrula and formed a well-organized shell in the D-veliger stage.

4.3. Functional analysis of *CgTyrp-2* and *CgTyr* in shell formation

Recent genomic and transcriptomic data show a substantial expansion of the tyrosinase family in *C. gigas* (Aguilera et al., 2014; Huang et al., 2017). In this study, we identified two tyrosinase genes (*CgTyr* and *CgTyrp-2*) belonging to the same family by analyzing data from NCBI. The protein sequence contains a typical tyrosinase structural domain with two copper binding sites, Cu(A) and Cu(B), featuring two conserved H-X(8)-H-x(8)-H motifs and an H-X(3)-Hx(22)-H motif (Decker and Tuzcek, 2000). This domain was also present in other type III copper-binding proteins, such as phenol oxidase, catechol oxidase, and heme glycosides, indicating that tyrosinase-like protein genes as a phenol oxidase (García-Borrón and Solano, 2002). Based on the peptide positions and conserved residues in the copper binding site, tyrosinases have been classified into three subclasses: secretory (A), cytoplasmic (B), and membrane-bound (C) (Furuhashi et al., 2009). In this study, *CgTyr* and *CgTyrp-2* contained transmembrane structural domains and were classified by the type-A. This type of tyrosinase can promote chitin deposition and formation by cross-linking o-diphenol and quinone tannins to form periostracum (Nagai et al., 2007).

To investigate the role of *CgTyr* and *CgTyrp-2* in larval shell formation, the CRISPR/Cas9 system was employed to individually knockout *CgTyr* or *CgTyrp-2*, and co-knockout *CgTyr* and *CgTyrp-2*. Deletion of *CgTyrp-2* or *CgTyr* results in delayed CaCO₃ deposition during larval shell formation, which was especially evident when both genes were co-knocked out. The formation of His-Cys cross-links in the active site is usually autocatalyzed, whereas copper is usually present in the active site of the enzyme (Nagai et al., 2007). The selected targets were located at the anterior structural domains of *CgTyr* or *CgTyrp-2*, resulting in targeted mutations that disrupt the activity of the copper-binding site, thereby affecting its affinity for substrate binding and thus the formation of the InCaS (Decker and Tuzcek, 2000). This disruption of the InCaS growth process further affected the formation of calcified shells. Additionally, the deletion of *CgTyrp-2* or *CgTyr* caused a significant increase in the mRNA expression of *CgChit4* and a decrease in *CgChs1* mRNA expression. Chitinase and chitin synthase played essential roles in the degradation and synthesis of chitin, respectively (Furuhashi et al., 2009) (Weiss and Schönitzer, 2006). Chitin was a critical component of molluscan shell structure and provided a framework for other macromolecules and guided the calcification process of crystal polymorphism (Furuhashi et al., 2009). Meanwhile, chitin was also the primary component of the larvae shell matrix, with varying content during larval development (Weiss and Schönitzer, 2006). Notably, pearl oyster chitinase was mainly expressed at the trochophore stage and in all the tissues studied, with the highest level in the mantle, particularly showing strong hybridization signals in the mantle edge (Li et al., 2017). Overall, the results suggested that tyrosinase deficiency impacts chitin synthesis, highlighting the importance of tyrosinase in the tanning of periosteal proteins. Interestingly, within the *CgTyrp-2* mutant group, where *CgTyrp-2* expression was down-regulated, a tendency for increased *CgTyr* expression was observed, and the reverse was not observed. We showed that it may be attributed to distinct patterns of *CgTyrp-2* and *CgTyr* gene expression during embryonic development. While gene expression levels, mRNA expression levels, and phenotypic results collectively suggest the involvement of *CgTyr* and *CgTyrp-2* in the calcification process during the early stages of oyster shell formation, it is imperative to acknowledge that further validation is essential to elucidate the molecular intricacies of calcification.

Prior investigations documented the concurrent modulation of multiple genes through the utilization of distinct sgRNAs targeting various genes (Wang et al., 2013; Liu et al., 2018). In this study, we co-injected Cas9/*CgTyrp-2* and *CgTyr* sgRNAs into fertilized eggs and showed success in oysters carrying both target mutations. Concurrently, our scrutiny of potential off-target sites for *CgTyrp-2* and *CgTyr* sgRNAs did not reveal any discernible mutations at these locations. We posited that the adoption of relatively low concentrations of sgRNA and Cas9 mRNA could potentially mitigate off-target effects, as they were degraded upon binding to target genes (Cai et al., 2018).

4.4. How to choose effective target sites

The success of CRISPR/Cas9 experiments relied heavily on the selection of appropriate sgRNAs, as the combination of sgRNA species, location and number can significantly affect the knockout efficiency (Haessler and Concordet, 2016). Rapid developments in bioinformatics tools have accelerated the quick application of CRISPR/Cas9, particularly due to the design of optimal and highly specific gRNA and post-genome-editing result analysis (Giner et al., 2023). However, there is still a lack of computational tools that strike an optimal balance between off-target and on-target effects (Naeem and Alkhnabashi, 2023). In this study, we tested five sgRNAs for *CgTyrp-2* and three sgRNAs for *CgTyr* using CRISPOR tool and found that four of the sequencing results showed high indel efficiency. This suggests that even the most optimized CRISPOR algorithmic tools currently in use for calculating gRNA on-target activity may exhibit certain limitations. Additionally, the location of the sgRNA could influence whether a knockout phenotype can be

observed (Shi et al., 2015). In *CgTyrp-2*, the designed sgRNAs were located at different positions, *CgTyrp-2*-sgRNA-64 located upstream of the Cu²⁺ structural domain and *CgTyrp-2*-sgRNA-54/12 located within the Cu²⁺ structural domain downstream. We also tested the knockout efficiencies of *CgTyrp-2*-sgRNA-64, *CgTyrp-2*-sgRNA-12, and *CgTyrp-2*-sgRNA-54 separately, and found that the knockout efficiency of *CgTyrp-2*-sgRNA-54 was highest. The knockout effects of the three sgRNA methods exhibited no significant distinctions in terms of phenotype.

Currently, the single gene is edited by multiple sgRNAs simultaneously, which can lead to the deletion of large gene segments (Ogawa et al., 2015; Yuan et al., 2019). For instance, a double sgRNA system is used to generate large biallelic gene deletions in rabbits that result in an albino phenotype (Yuan et al., 2019). To validate large DNA fragment deletions, we selected two sgRNA targets within *CgTyrp-2*: one situated in the 5'UTR of *CgTyrp-2* and the other within exon four. When both sgRNAs were employed simultaneously, the anticipated outcome was the recurrent deletion of a fragment. However, if only one sgRNA was active, deletion of varying lengths, ranging from 2 to 16 base pairs, occurred. Our results demonstrate the precision and efficiency of gene deletions, with deletions spanning up to 2 kb at the designated locus. These findings suggest that such substantial block deletions have the potential to yield more pronounced knockout phenotypes when compared to alternative models. This marks the inaugural account of generating sizeable two-copy gene deletions within oysters through a dual sgRNA system and cytoplasmic microinjection. This underscores the system's potential effectiveness not only in cellular and model animal contexts but also within oysters.

However, our results showed that the efficiency of large deletions in oysters was currently suboptimal. This inefficiency can be attributed to the dependence of site-specific cleavage on the concentration of both sgRNA and the Cas9 endonuclease (Li et al., 2021; Yu et al., 2019). Based on the findings, we formulated the hypothesis that the limited efficacy observed during the simultaneous injection of multiple sgRNAs could stem from a scenario wherein numerous sgRNAs and gene target sites compete for access to the same Cas9 enzyme. Hence, it has become imperative to strategically enhance the efficiency of our approach. This can be achieved through the meticulous optimization of critical variables such as the concentration of Cas9/sgRNA complexes, the number of sgRNA molecules, the precise gene target locus, as well as the GC content within the designed sgRNAs (Oo et al., 2020).

Ethics statement

The experiments in this study were conducted according to institutional and national guidelines, in line with the ARRIVE guidelines and in accordance with the UK Animals (Scientific Procedures) Act 1986 and related guidelines, the EU Directive 2010/63/EU on experiments on animals, or the U.S. National Research Council's Guide for the Care and Use of Laboratory Animals. No endangered or protected species was involved in the experiments of the study. No specific permission was required for the location of the culture experiment. During the experimental process, we used mature male and female oysters to do in vitro fertilization and observed the early development of the embryo, and all the experimental operations were in accordance with the management and technical specifications of animal experiments.

CRedit authorship contribution statement

Qian Li: Writing – original draft, Software, Methodology, Investigation, Formal analysis, Data curation. **Hong Yu:** Writing – review & editing, Supervision, Methodology. **Qi Li:** Writing – original draft, Software, Methodology, Investigation, Formal analysis, Data curation.

Declaration of competing interest

The authors declare that they have no known competing financial

interests or personal relationships that could have appeared to influence the work reported in this paper.

Data availability

Data will be made available on request.

Acknowledgments

This work was supported by grants from the National Key R&D Program of China (2022YFD2400305), Earmarked Fund for Agriculture Seed Improvement Project of Shandong Province (2022LZGCQY010, 2021LZGC027 and 2021LZGX03), and China Agriculture Research System Project (CARS-49).

Appendix A. Supplementary material

Supplementary data to this article can be found online at <https://doi.org/10.1016/j.gene.2024.148748>.

References

- Abblain, J., Durand, E.M., Yang, S., Zhou, Y., Zon, L.I., 2015. A CRISPR/Cas9 vector system for tissue-specific gene disruption in zebrafish. *Dev. Cell* 32, 756–764.
- Addadi, L., Joester, D., Nudelman, F., Weiner, S., 2006. Mollusk shell formation: A source of new concepts for understanding biomineralization processes. *Chem. Eur. J.* 12, 980–987.
- Aguilera, F., McDougall, C., Degnan, B.M., 2014. Evolution of the tyrosinase gene family in bivalve molluscs: Independent expansion of the mantle gene repertoire. *Acta Biomater.* 10, 3855–3865.
- Aranda-Burgos, J.A., Da Costa, F., Novoa, S., Ojea, J., Martinez-Patino, D., 2014. Embryonic and larval development of *Ruditapes decussatus* (Bivalvia: Veneridae): A study of the shell differentiation process. *J. Mollus. Stud.* 80, 8–16.
- Arivalagan, J., Yarra, T., Marie, B., Sleight, V.A., Duvernois-Berthet, E., Clark, M.S., Marie, A., Berland, S., 2017. Insights from the shell proteome: biomineralization to adaptation. *Mol. Biol. Evol.* 34, 66–77.
- Bai, M., Liang, D., Wang, Y., Li, Q., Wu, Y., Li, J., 2016. Spermatogenic cell-specific gene mutation in Mice via CRISPR-Cas9. *J. Genet. Genomics* 43, 289–296.
- Cai, Y., Chen, L., Sun, S., Wu, C., Yao, W., Jiang, B., Han, T., Hou, W., 2018. CRISPR/Cas9-mediated deletion of large genomic fragments in Soybean. *Int. J. Mol. Sci.* 19, 3835.
- Chang, T.-S., 2009. An updated review of tyrosinase inhibitors. *Int. J. Mol. Sci.* 10, 2440–2475.
- Chen, X., Liu, X., Bai, Z., Zhao, L., Li, J., 2017. *HcTyr* and *HcTyp-1* of *Hyriopsis cumingii*, novel tyrosinase and tyrosinase-related protein genes involved in nacre color formation. *Comp. Biochem. Physiol. B Biochem. Mol. Biol.* 204, 1–8.
- Conant, D., Hsiau, T., Rossi, N., Oki, J., Maures, T., Waite, K., Yang, J., Joshi, S., Kelso, R., Holden, K., Enzmann, B.L., Stoner, R., 2022. Inference of CRISPR edits from sanger trace data. *CRISPR J.* 5, 123–130.
- De Wit, P., Durland, E., Ventura, A., Langdon, C.J., 2018. Gene expression correlated with delay in shell formation in larval Pacific oysters (*Crassostrea gigas*) exposed to experimental ocean acidification provides insights into shell formation mechanisms. *BMC Genom.* 19, 160.
- Decker, H., Tuzek, F., 2000. Tyrosinase/catecholoxidase activity of hemocyanins: structural basis and molecular mechanism. *Trends Biochem. Sci.* 25, 392–397.
- Du, Y., Zhang, L., Xu, F., Huang, B., Zhang, G., Li, L., 2013. Validation of housekeeping genes as internal controls for studying gene expression during Pacific oyster (*Crassostrea gigas*) development by quantitative real-time PCR. *Fish & Shellfish Immunol.* 34, 939–945.
- Edgar, A., Byrne, M., Wray, G.A., 2019. Embryo microinjection of the lecithotrophic sea urchin *Heliocidaris erythrogramma*. *J. Biol. Methods* 6, e119.
- Edwards, R.B., Leininger, S., Kleppe, L., Skafnesmo, K.O., Wargelius, A., 2014. Kleppe, K.O. Skafnesmo, A. Wargelius. Targeted mutagenesis in Atlantic Salmon (*Salmo salar L.*) using the CRISPR/Cas9 system induces complete knockout individuals in the F0 generation. *PLoS One* 9, e108622.
- Feng, D., Li, Q., Yu, H., Zhao, X., Kong, L., 2015. Comparative transcriptome analysis of the Pacific oyster *Crassostrea gigas* characterized by shell colors: Identification of genetic bases potentially involved in pigmentation. *PLoS One* 10, e0145257.
- Feng, D., Li, Q., Yu, H., Kong, L., Du, S., 2017. Identification of conserved proteins from diverse shell matrix proteome in *Crassostrea gigas*: characterization of genetic bases regulating shell formation. *Sci. Rep.* 7, 45754.
- Feng, D., Li, Q., Yu, H., 2019. RNA interference by ingested dsRNA-expressing bacteria to study shell biosynthesis and pigmentation in *Crassostrea gigas*. *Mar. Biotechnol.* 21, 526–536.
- Furuhashi, T., Schwarzinger, C., Miksik, I., Smrz, M., Beran, A., 2009. Molluscan shell evolution with review of shell calcification hypothesis. *Comp. Biochem. Physiol. B: Biochem. Mol. Biol.* 154, 351–371.
- Gandhi, S., Haeussler, M., Razy-Krajka, F., Christaen, L., Stolfi, A., 2017. Evaluation and rational design of guide RNAs for efficient CRISPR/Cas9-mediated mutagenesis in *Ciona*. *Dev. Biol.* 425, 8–20.
- García-Borrón, J.C., Solano, F., 2002. Molecular anatomy of tyrosinase and its related proteins: Beyond the histidine-bound metal catalytic center. *Pigm. Cell* 15, 162–173.
- Giner, G., Ikram, S., Herold, M.J., Papenfuss, A.T., 2023. A systematic review of computational methods for designing efficient guides for CRISPR DNA base editor systems. *Brief. Bioinform.* 24, bbad205.
- Haeussler, M., Concordet, J.-P., 2016. Genome editing with CRISPR-Cas9: Can it get any better. *J. Genet. Genomics* 43, 239–250.
- Huan, P., Liu, G., Wang, H., Liu, B., 2013. Identification of a tyrosinase gene potentially involved in early larval shell biogenesis of the Pacific oyster *Crassostrea gigas*. *Dev. Genes Evol.* 223, 389–394.
- Huan, P., Cui, M., Wang, Q., Liu, B., 2021. CRISPR/Cas9-mediated mutagenesis reveals the roles of calaxin in gastropod larval cilia. *Gene* 787, 145640.
- Huang, R., Li, L., Zhang, G., 2017. Structure-based function prediction of the expanding mollusk tyrosinase family. *Chin. J. Ocean. Limnol.* 35, 1454–1464.
- Jiang, K., Jiang, L., Nie, H., Huo, Z., Yan, X., 2020. Molecular cloning and expression analysis of tyrosinases (*tyr*) in four shell-color strains of Manila clam *Ruditapes philippinarum*. *PeerJ* 8, e8641.
- Kurita, Y., Deguchi, R., Wada, H., 2009. Early development and cleavage pattern of the Japanese purple mussel, *Septifer virgatus*. *Zool. Sci.* 26, 814–820.
- Lee, S.H., Kim, S.R., Park, C.H., Cho, S.J., Choi, Y.H., 2006. Loss of heterozygosity of chromosome 17p13 and p53 expression in invasive ductal carcinomas. *J. Breast Cancer* 9, 309.
- Li, H., Wang, D., Deng, Z., Huang, G., Fan, S., Zhou, D., Liu, B., Zhang, B., Yu, D., 2017. Molecular characterization and expression analysis of chitinase from the pearl oyster *Pinctada fucata*. *Comp. Biochem. Phys. B* 203, 141–148.
- Li, H., Yu, H., Li, Q., 2021. Striated myosin heavy chain gene is a crucial regulator of larval myogenesis in the Pacific oyster *Crassostrea gigas*. *Int. J. Biol. Macromol.* 179, 388–397.
- Li, H., Yu, H., Du, S., Li, Q., 2021. CRISPR/Cas9 mediated high efficiency knockout of myosin essential light chain gene in the Pacific oyster (*Crassostrea gigas*). *Mar. Biotechnol.* 23, 215–224.
- Liao, Z., Bao, L., Fan, M., Gao, P., Wang, X., Qin, C., Li, X., 2015. In-depth proteomic analysis of nacre, prism, and myostracum of *Mytilus* shell. *J. Proteomics* 122, 26–40.
- Liu, Q., Qi, Y., Liang, Q., Song, J., Liu, J., Li, W., Shu, Y., Tao, M., Zhang, C., Qin, Q., Wang, J., Liu, S., 2019. Targeted disruption of tyrosinase causes melanin reduction in *Carassius auratus cuvieri* and its hybrid progeny. *Sci. China Life Sci.* 62, 1194–1202.
- Liu, H., Sui, T., Liu, D., Liu, T., Chen, M., Deng, J., Xu, Y., Li, Z., 2018. Multiple homologous genes knockout (KO) by CRISPR/Cas9 system in rabbit. *Gene* 647, 261–267.
- Luo, Y.-J., Takeuchi, T., Koyanagi, R., Yamada, L., Kanda, M., Khalturina, M., Fujie, M., Yamasaki, S., Endo, K., Satoh, N., 2015. The *Lingula* genome provides insights into brachiopod evolution and the origin of phosphate biomineralization. *Nat. Commun.* 6, 8301.
- Mann, S., 1988. Molecular recognition in biomineralization. *Nature* 332, 119–124.
- Marin, F., 2012. The formation and mineralization of mollusk shell. *Front Biosci.* S4, 1099–1125.
- Miglioli, A., Dumollard, R., Balbi, T., Besnardeau, L., Canesi, L., 2019. Characterization of the main steps in first shell formation in *Mytilus galloprovincialis*: Possible role of tyrosinase. *Proc. R. Soc. B* 286, 20192043.
- Min, Y., Li, Q., Yu, H., 2022. Heme-peroxidase 2 modulated by POU2F1 and SOX5 is involved in pigmentation in Pacific oyster (*Crassostrea gigas*). *Mar. Biotechnol.* 24, 263–275.
- Miyazaki, Y., Nishida, T., Aoki, H., Samata, T., 2010. Expression of genes responsible for biomineralization of *Pinctada fucata* during development. *Comp. Biochem. Physiol. B: Biochem. Mol. Biol.* 155, 241–248.
- Moueza, M., Gros, O., Frenkiel, L., 2006. Embryonic development and shell differentiation in *Chione cancellata* (Bivalvia, Veneridae): an ultrastructural analysis. *Invertebr. Biol.* 125, 21–33.
- Naem, M., Alkhnbashi, O.S., 2023. Current bioinformatics tools to optimize CRISPR/Cas9 experiments to reduce off-target effects. *Int. J. Mol. Sci.* 24, 6261.
- Nagai, K., Yano, M., Morimoto, K., Miyamoto, H., 2007. Tyrosinase localization in mollusc shells. *Comp. Biochem. Physiol. B: Biochem. Mol. Biol.* 146, 207–214.
- Nudelman, F., Gotliv, B.A., Addadi, L., Weiner, S., 2006. Mollusk shell formation: Mapping the distribution of organic matrix components underlying a single aragonitic tablet in nacre. *J. Struct. Biol.* 153, 176–187.
- Ogawa, T., Iwata, T., Kaneko, S., Itaya, M., Hirota, J., 2015. An inducible *recA* expression *Bacillus subtilis* genome vector for stable manipulation of large DNA fragments. *BMC Genom.* 16, 209.
- Oo, Z.M., Adlat, S., Sah, R.K., Myint, M.Z.Z., Hayel, F., Chen, Y., Htoo, H., Bah, F.B., Bahadar, N., Chan, M.K., Zhang, L., Feng, X., Zheng, Y., 2020. Brain transcriptome study through CRISPR/Cas9 mediated mouse *Dip2c* gene knock-out. *Gene* 758, 144975.
- Ramesh, K., Yarra, T., Clark, M.S., John, U., Melzner, F., 2019. Expression of calcification-related ion transporters during blue mussel larval development. *Ecol. Evol.* 9, 7157–7172.
- Ren, G., Chen, C., Jin, Y., Zhang, G., Hu, Y., Shen, W., 2020. A novel tyrosinase gene plays a potential role in modification of the shell organic matrix of the triangle mussel *Hyriopsis cumingii*. *Front. Physiol.* 11, 100.
- Rose, R.A., Baker, S.B., 1994. Larval and spat culture of the Western Australian silver- or goldlip pearl oyster, *Pinctada maxima Jameson* (Mollusca: Pteriidae). *Aquaculture* 126, 35–50.

- Shi, J., Wang, E., Milazzo, J.P., Wang, Z., Kinney, J.B., Vakoc, C.R., 2015. Discovery of cancer drug targets by CRISPR-Cas9 screening of protein domains. *Nat. Biotechnol.* 33, 661–667.
- Song, X., Liu, Z., Wang, L., Song, L., 2019. Recent advances of shell matrix proteins and cellular orchestration in marine molluscan shell biomineralization. *Front. Mar. Sci.* 6, 41.
- Sun, D., Yu, H., Li, Q., 2023. Examination of the role of *CgSox-like* in sex determination and gonadal development in the Pacific oyster *Crassostrea gigas*. *Aquaculture* 566, 739234.
- Suzuki, M., Saruwatari, K., Kogure, T., Yamamoto, Y., Nishimura, T., Kato, T., Nagasawa, H., 2009. An acidic matrix protein, *Pif*, is a key macromolecule for nacre formation. *Science* 325, 1388–1390.
- Ventura, A., Schulz, S., Dupont, S., 2016. Maintained larval growth in mussel larvae exposed to acidified under-saturated seawater. *Sci. Rep.* 6, 23728.
- Wang, H., Yang, H., Shivalila, C.S., Dawlaty, M.M., Cheng, A.W., Zhang, F., Jaenisch, R., 2013. One-step generation of mice carrying mutations in multiple genes by CRISPR/Cas-mediated genome engineering. *Cell* 153, 910–918.
- Weiss, I.M., Schönitzer, V., 2006. The distribution of chitin in larval shells of the bivalve mollusk *Mytilus galloprovincialis*. *J. Struc.* 153, 264–277.
- Yang, W., Huan, P., Liu, B., 2020. Early shell field morphogenesis of a patellogastropod mollusk predominantly relies on cell movement and F-actin dynamics. *BMC Dev. Biol.* 20, 18.
- Yang, B., Pu, F., Li, L., You, W., Ke, C., Feng, D., 2017. Functional analysis of a tyrosinase gene involved in early larval shell biogenesis in *Crassostrea angulata* and its response to ocean acidification. *Comp. Biochem. Physiol. B: Biochem. Mol. Biol.* 206, 8–15.
- Yao, H., Cui, B., Li, X., Lin, Z., Dong, Y., 2020. Characteristics of a novel tyrosinase gene involved in the formation of shell color in hard clam *Meretrix meretrix*. *J. Ocean Univ. China* 19, 183–190.
- Yu, H., Li, H., Li, Q., Xu, R., Yue, C., Du, S., 2019. Targeted gene disruption in Pacific oyster based on CRISPR/Cas9 ribonucleoprotein complexes. *Mar. Biotechnol.* 21, 301–309.
- Yuan, T., Zhong, Y., Wang, Y., Zhang, T., Lu, R., Zhou, M., Lu, Y., Yan, K., Chen, Y., Hu, Z., Liang, J., Fan, J., Cheng, Y., 2019. Generation of hyperlipidemic rabbit models using multiple sgRNAs targeted CRISPR/Cas9 gene editing system. *Lipids Health Dis.* 18, 69.
- Zaidi, K.U., Ali, S.A., Ali, A.S., 2016. Effect of purified mushroom tyrosinase on melanin content and melanogenic protein expression. *Biotech. Res. Int.* 1–8.
- Zhao, R., Takeuchi, T., Luo, Y.-J., Ishikawa, A., Kobayashi, T., Koyanagi, R., Villar-Briones, A., Yamada, L., Sawada, H., Iwanaga, S., Nagai, K., Satoh, N., Endo, K., 2018. Dual gene repertoires for larval and adult shells reveal molecules essential for molluscan shell formation. *Mol. Biol. Evol.* 11, 2751–2761.
- Zhu, Y., Li, Q., Yu, H., Liu, S., Kong, L., 2021. Shell biosynthesis and pigmentation as revealed by the expression of tyrosinase and tyrosinase-like protein genes in Pacific oyster (*Crassostrea gigas*) with different shell colors. *Mar. Biotechnol.* 23, 777–789.
- Zhu, Y., Li, Q., Yu, H., Liu, S., Kong, L., 2022. Expression of tyrosinase-like protein genes and their functional analysis in melanin synthesis of Pacific oyster (*Crassostrea gigas*). *Gene* 840, 146742.